Geophysical Journal International

Geophys. J. Int. (2011) **185,** 724–736 doi: 10.1111/j.1365-246X.2011.04958.x

Slip distribution beneath the Central and Western Himalaya inferred from GPS observations

M. Ponraj,[1] S. Miura,[2] C. D. Reddy,[1] S. Amirtharaj[1] and S. H. Mahajan[1]

[1] *Indian Institute of Geomagnetism, New Panvel, Navi Mumbai*-410218, *India. E-mail: pon@iigs.iigm.res.in*
[2] *Graduate School of Science, Tohoku University, Aoba-ku, Sendai*-9808578, *Japan*

Accepted 2011 January 17. Received 2010 December 28; in original form 2010 May 5

SUMMARY

Underthrusting of the Indian Plate beneath the Himalaya has been the cause of many hazardous thrust-faulting earthquakes along the arc. Moderate earthquakes with magnitudes of $\leq$5 occur frequently in this region, releasing the elastic strain accumulated over many years around the plate boundary. These events can be attributed to slip deficits where the Indian and Eurasian Plates are locked during interseismic periods. Geodetic measurements can help discriminate the distribution of the interlocking areas and the steadily slipping areas beneath the Himalaya. To understand the deformation across the Central and Western Himalaya and the associated slip on thrust faults, campaign-mode GPS data were collected in the Garhwal–Kumaun region of the Western Himalaya. GPS sites velocities show that the deformation is currently concentrated between the Lesser and Higher Himalaya. Horizontal velocities are used to estimate the slip distribution. For the estimation, a model of the interseismic surface deformation caused by buried non-uniform creep dislocation (NUC) on a curved fault surface is used. The slip distribution shows that there might be structural discontinuity on the fault between the Kumaun and Garhwal regions of the Himalaya. The estimated slip rate at the depth around 20–40 km in the Central Himalaya and at the depth of ~15 km in the Western Himalaya is 10 mm yr^{-1}. The NUC model indicates that the shallow part (<20 km) of the thrust fault system along the plate boundary is almost locked. The locking depth appears to be deep in the Central Himalaya and shallower in the Western Himalaya. Further, most of the historical large seismic events are observed to have occurred in an area with a slip velocity less than 10 mm yr^{-1} (i.e. in a locked zone) at the plate interface.

Key words: Satellite geodesy; Creep and deformation; Seismicity and tectonics; Kinematics of crustal and mantle deformation.

1 INTRODUCTION

The continuous process of continent–continent collision between the Indian and Eurasian Plates has led to the formation of the Himalayan range, since ~50 Ma. This has contributed to the high elevation, fold-thrust formation and large crustal shortening along the ~2500-km-long stretch of the Himalayan arc (Molnar & Tapponnier 1977; Seeber *et al.* 1981; Srivastava & Mitra 1994). Three major south-verging thrust systems have developed along the length of the arc (Fig. 1). The northernmost fault is the Main Central Thrust (MCT), which emerges along the southern edge of the Higher Himalaya and separates the high-grade metamorphic rocks of the High Himalayan Crystalline Sequence from the weakly metamorphosed series of the Lesser Himalaya (Nakata 1989). The Main Boundary Thrust (MBT) marks the southern edge of the Lesser Himalaya and forms a series of north-dipping thrust faults, and it separates the low-grade metasediments of the Lesser Himalaya from the sandstones of the sub-Himalaya. The southernmost fault is the Main Frontal Thrust (MFT), which is considered to be the most active of the three faults, and bounds the northern limit of the exposed Indian Plate.

The Indian Plate continues to move northeastward and to converge with the Eurasian Plate at the rate of ~50 mm yr^{-1} (Patriat & Achache 1984; Bilham *et al.* 1997; Larson *et al.* 1999). Geological and seismological evidences suggest that the convergence rate in the Himalaya is ~20 mm yr^{-1} (Molnar & Deng 1984; Armijo *et al.* 1986; Molnar & Lyon-Caen 1989; Bilham *et al.* 1997). Of the total convergence, ~50 per cent occurs in the Himalaya, and the remaining involves distributed deformation (Demets *et al.* 1994; England & Molnar 1997; Holt *et al.* 2000; Wang *et al.* 2001; Chen *et al.* 2004a,b). The focal mechanism solution (Molnar & Lyon-Caen 1989) suggests that the convergence axis rotates counter-clockwise from west to east in the arc-perpendicular direction. This is consistent with the east–west hangingwall extension across southern Tibet (Armijo *et al.* 1986; Larson *et al.* 1999).

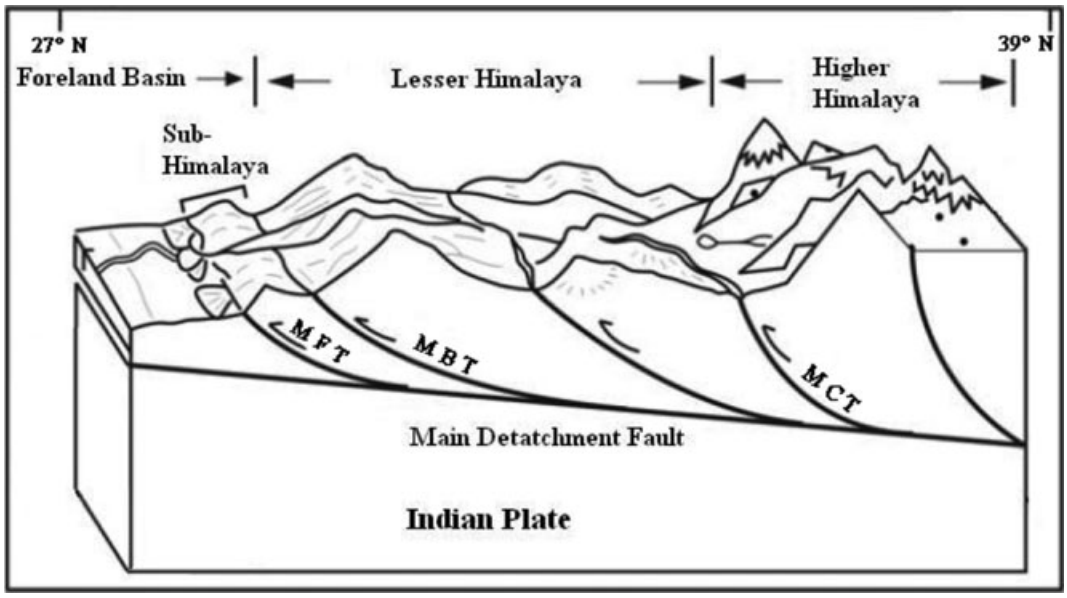

Figure 1. Schematic representation of the fault system beneath the Himalaya (modified after Gansser 1964). MCT: Main Central Thrust; MBT: Main Boundary Thrust; MFT: Main Frontal Thrust.

Moderate to large earthquakes that have occurred along the Himalayan arc are shown in Fig. 2. The rupture zone between two great earthquakes, namely, the 1905 Kangra earthquake (M 7.8) and the 1934 Bihar–Nepal earthquake (M 8.1), is referred to as the seismic gap and is ∼800 km in length (Khattri 1987; Bilham 1995). This zone is considered to be a potential source of large earthquakes (Bilham *et al.* 2001). These earthquakes cause a slip on the MFT along the Himalayan arc and can be attributed to slip deficits on the locked plate boundary (Pandey & Molnar 1988; Ambraseys & Bilham 2000). It is important to understand the present-day deformation to asses the seismic hazard of this area. The Global Positioning System (GPS) technique is an effective and unique tool to precisely measure deformation along individual thrust faults; such measurements are valuable for understanding the convergence between the Indian and Eurasian Plates.

2 GPS DATA ANALYSIS AND RESULTS

A GPS network was established in the Kumaun region (Fig. 3) of the Western Himalaya in 2005 May. At each site, a concrete pillar was constructed, and a non-magnetized steel plate was fixed over the pillar to settle a GPS antenna. GPS measurements commenced in 2005 December, and campaign measurements have been repeated every year since then. We tried to obtain GPS data during the winter season so as to avoid seasonal variations. We also collected GPS data from the Garhwal Himalaya (west of the Kumaun Himalaya) during 1999–2003, after the 1999 Chamoli earthquake (M 6.9). The locations of the GPS sites and the observation times are listed in Table 1. Trimble 4000SSE receivers were used for the observations; in addition, choke ring antennas with Dorne Margolin elements were used to reduce multipath effects on the signal. Also, a satellite elevation cut-off angle of 15° was used to reduce multipath effects. All the stations were continuously operated for three to four days, and the sampling interval was 30 seconds. We analysed the GPS data together with data from some IGS fiducial sites by using the GAMIT/GLOBK (King & Bock 2005) post-processing software. Double-difference GPS phase observations were used to estimate the station coordinates, receiver clock parameters, atmospheric zenith delay and horizontal delay gradients and orbital and Earth rotation parameters. To reduce errors in the GPS-derived positions, the solid Earth tides and the ocean loading effect were taken into account by using the global tide model FES2004 (Lyard *et al.* 2006; Vergnolle *et al.* 2008).

To obtain the GPS site coordinates and velocities with reference to ITRF2000 (Altamimi *et al.* 2002), loosely constrained daily solutions were combined with the permanent tracking solutions of the IGS stations (Herring 2002). We determined the weights for each set of combined quasi-observations by adjusting the chi-square increments per degree of freedom through both forward and backward filtering of data to achieve the optimum value for the repeatability of the coordinates (McClusky *et al.* 2000).

Estimated ITRF2000 velocities of GPS stations are converted to velocities in the fixed Indian frame by using the Euler pole (52.970°N, –0.297°E with angular velocity of 0.499° Myr^{-1}) of relative motion defined by Banerjee *et al.* (2008). Velocity vectors with respect to the Indian Plate are shown in Fig. 3. Times-series of estimated site coordinates at some of the stations in the GPS network are shown in Fig. 4.

From the velocities with respect to the Indian frame, it can be seen that sites near the MCT show more variations than the stations near the MBT and MFT. This may suggest that the updip of the plate interface is locked beneath the study area. The zone with the maximum convergence rate, which accommodates much of the shortening, is well north of the frontal thrust system, and the convergence rate is comparable to the geological slip rate over the last few million years (Lav'e & Avouac 2000); further, the MFT is locked (Bilham *et al.* 1997; Larson *et al.* 1999; Jouanne *et al.* 1999, 2004). It is also observed that DHAR is moving southward while MUNS is moving northwestward. A cluster of microseismicity (Fig. 3) can be seen to the southeast and northwest of MUNS. The activity of microseismicity is relatively low and non-homogeneously distributed in the region (Tsapanos 1990; Wason *et al.* 2002; Khan & Chakaraborthy 2007). The region MUNS situated may be high strength homogeneity.

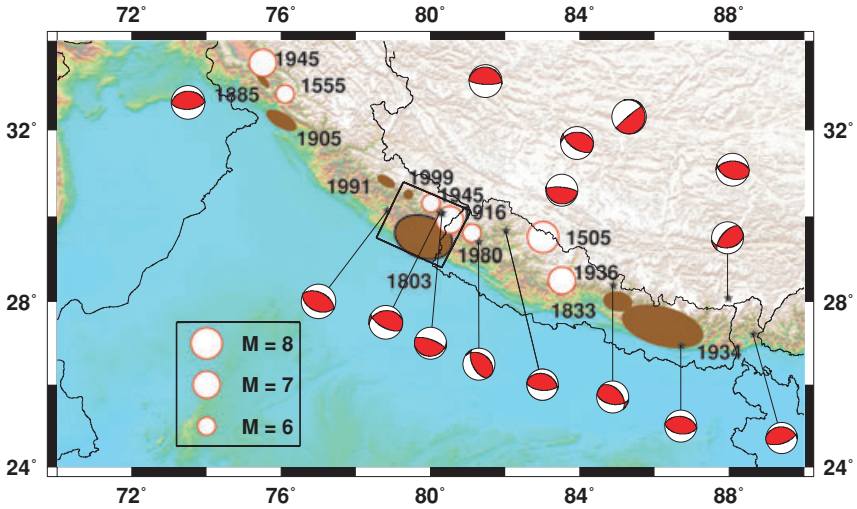

Figure 2. Epicentres of historical earthquakes that have occurred along the Himalayan arc (shown as open circles along with the year of occurrence). The small rectangular is the location of the GPS observational network in the Kumaun–Garhwal region established by the present study. Focal mechanisms of the earthquakes that occurred during the GPS data collection period (2005–2007) are shown (Harvard CMT database). The brown hatched areas indicate the ruptures of large earthquakes (adapted from Bilham *et al.* 2001).

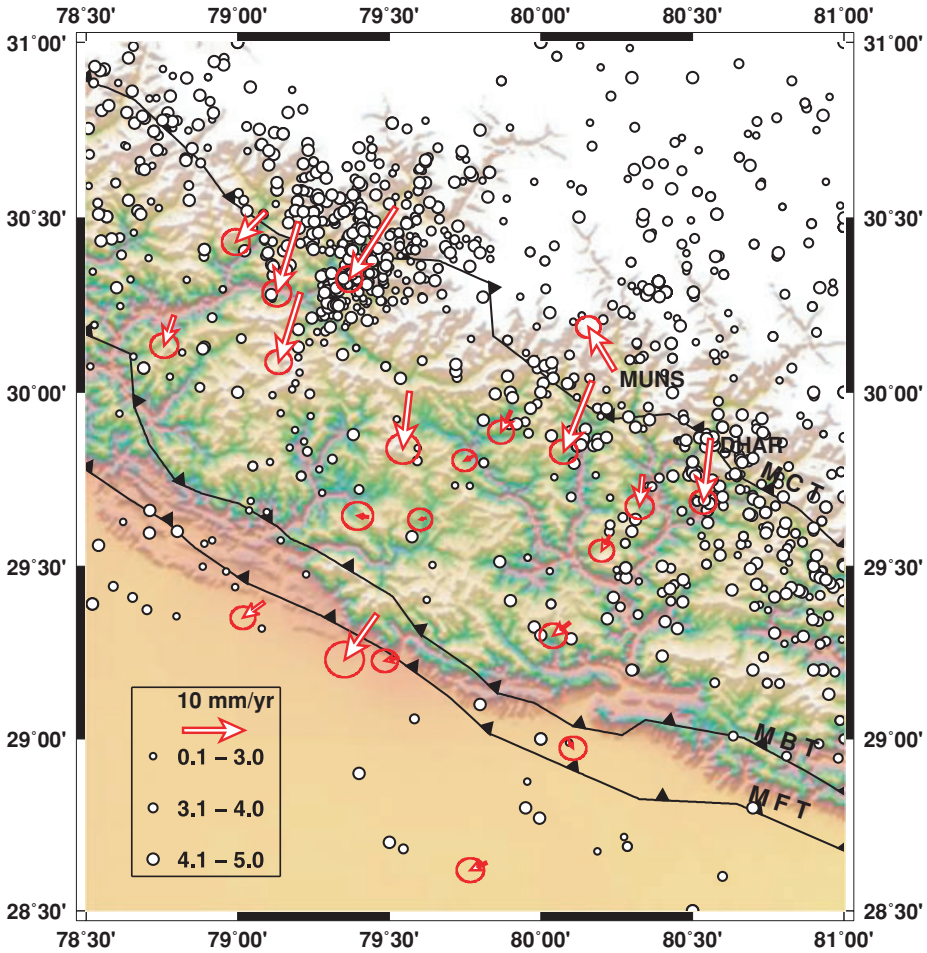

Figure 3. Estimated site velocities at our GPS stations in the Kumaun–Garhwal Himalaya with respect to the fixed Indian frame. The epicentres of the earthquakes (focal depth < 50 km) are shown as open circles (downloaded from http://www.iris.edu/data/event/eventsearch.html). Lines with triangles denote the Main Central Thrust (MCT), Main Boundary Thrust (MBT) and Main Frontal Thrust (MFT).

Table 1. GPS-derived horizontal velocities with respect to ITRF 2000 and the Indian fixed frame.

			Observation period in DOY taken			Velocities with respect to ITRF 2000				Velocities with respect to Indian frame			
Site code	Latitude (°N)	Longitude (°E)	2005	2006	2007	East rate mm yr^{-1}	North rate mm yr^{-1}	σE mm yr^{-1}	σN mm yr^{-1}	East rate mm yr^{-1}	North rate mm yr^{-1}	σE mm yr^{-1}	σN mm yr^{-1}
RAMR	29.23	79.08	341–344	307–310	323–327	36.30	31.03	0.74	0.67	−0.34	−2.48	0.74	0.67
HALD	29.21	79.51	346–350	307–310	322–327	34.67	34.03	0.78	0.67	−2.15	0.52	0.78	0.67
PILI	28.63	79.85	343–345	308–311	324–328	33.52	32.36	0.82	0.71	−3.59	−1.15	0.82	0.71
BANB	29.10	80.18	342–344	308–311	323–328	37.81	32.15	0.80	0.69	0.74	−1.35	0.80	0.69
PITH	29.59	80.23	351–354	313–316	329–336	35.60	31.11	0.74	0.65	−1.30	−2.39	0.74	0.65
CHAM	29.33	80.09	351–354	313–316	336–339	34.21	31.41	0.81	0.73	−2.74	−2.09	0.81	0.73
ASKO	29.76	80.34	–	315–317	329–334	37.35	28.37	0.84	0.74	0.48	–5.13	0.84	0.74
DHAR	29.86	80.56	353–356	315–317	330–334	38.10	23.29	0.80	0.71	1.20	–10.21	0.80	0.71
MUNS	30.06	80.20	355–358	319–322	334–340	32.59	39.18	0.73	0.64	−4.15	6.98	0.73	0.63
GIRG	30.03	80.17	–	319–322	335–338	29.19	30.43	0.82	0.72	−4.60	−11.4	0.82	0.72
BAGR	29.82	79.77	358–361	320–323	338–342	34.44	32.85	0.73	0.64	−1.25	−0.65	0.73	0.64
KAPK	29.78	79.90	360–362	324–327	341–345	35.04	30.11	0.77	0.69	−1.64	−3.39	0.77	0.69
ALMO	29.59	79.65	357–359	325–329	347–350	37.56	33.68	0.72	0.65	0.85	0.17	0.72	0.65
RANI	29.64	79.43	363–365 1999	326–328 2001	346–349 2003	34.88	33.78	0.93	0.83	−1.77	0.27	0.93	0.83
SRIN	78.790	30.219	181–184, 188,189	284–291	120–129	32.92	32.51	0.83	0.73	–2.31	–0.36	0.83	0.73
PAIN	79.520	30.529	184–185	289–290	126–127	28.13	21.22	0.78	0.77	−7.16	−11.7	0.78	0.77
KHAL	79.206	30.285	181–182	290–291	127–128	23.53	31.98	0.79	0.71	−0.35	−1.2	0.79	0.71
CHOP	79.200	30.487	188–190	285–286	122–123	24.94	34.21	0.86	0.79	−10.3	1.3	0.86	0.79
OKHI	79.091	30.517	189–190	285,286	124,125	28.14	31.06	0.83	0.73	−4.1	−4.8	0.83	0.73
HYDE	17.42	78.55	341–365	307–330	323–350	41.92	33.10	0.72	0.64	−1.49	−0.96	0.72	0.64
IISC	13.02	77.57	341–365	307–330	323–350	42.71	32.59	0.67	0.65	0.94	−1.95	0.67	0.65
MUMB	19.13	72.91	341–365	307–330	323–350	37.90	32.01	0.69	0.63	−0.92	−0.06	0.69	0.63

3 INVERSION APPROACH

Many authors (Vergne *et al.* 2001; Jouanne *et al.* 2004; Feldl & Bilham 2006; Bettinelli *et al.* 2006) have discussed the slip rate beneath the Himalaya by using creeping dislocation rather than the back slip model. These authors have assumed that the convergence rate is proportional to the creeping dislocation below the locked portion of the MFT. In the present study, the method devised by Yabuki & Matsu'ura (1992), which adopt Akaike's Bayesian Information Criterion (ABIC) to select a weighting coefficient for smoothness of slip distribution, is used to construct a model of the slip distribution on a curved fault surface. First, we try to understand the deformation in the Kumaun–Garhwal section, which lies close to the centre of the Himalayan fold and thrust belt. Then, we investigate the slip distribution beneath the Central and Western Himalaya by including GPS velocities for stations in Nepal (Central Himalaya) and the northwest Himalaya (Western Himalaya) obtained from the literature (Jade *et al.* 2004; Bettinelli *et al.* 2006; Banerjee *et al.* 2008). Velocity vectors with respect to the Indian frame are shown in Fig. 5.

3.1 Fault model

The fine subsurface structure was studied by deep crustal reflection seismic profiles of the region beneath the Greater and Tibetan Himalayan Zones in the INDEPTH project (Zhao *et al.* 1993; Nelson *et al.* 1996; Hauck *et al.* 1998). The fault geometry used in our analysis was obtained by considering their cross-sections of different observation lines presented in earlier studies (Jouanne *et al.* 2004; Yin 2006; Bettinelli *et al.* 2006). The assumed fault plane extends for 1700 km along strike (NE–SW direction) and 900 km along dip direction, and is meshed with 26 × 15 bicubic B-spline functions (Yabuki & Matsu'ura 1992). The plate interface was defined down to the depth of 120 km. We modelled the interseismic surface deformation in an elastic, homogeneous and isotropic half-space (Okada 1985) with a curved fault surface by using the buried non-uniform creep distribution (NUC) model (Fig. 6). We used ABIC approach, described by Yabuki & Matsu'ura (1992), to select the optimum values of the hyperparameter controlling the data fitness and the smoothness of the fault slip. For the best estimation of likelihood prior constraints by adjusting the hyperparameters were to get the minimum ABIC values, for achieving smooth distribution of fault slip model. Once the minimum ABIC values were obtained, the model parameters and covariance for the estimation errors were computed.

3.2 Resolution test

A resolution test was performed using slip patches of 30 mm (grey) and 0 mm (white) given on the fault plane shown in Fig. 7. The model is like Zebra test performed in the North Island subduction zone, New Zealand by Wallace *et al.* (2004). Slip patches were considered to be absent in the updip area of the fault model, since the plate interface of the MFT is locked. The random noise of standard deviation of 1.2 mm for horizontal component is added to the synthetic velocities at each site for the test. The result of the resolution test is shown in Fig. 7. The synthetic site velocities (Fig. 8) were reproduced fairly well. The locations of the areas of high slip matches the input model for the given slip distribution in the downdip portion, but it shows slightly less magnitude in the updip portion of the model. This shows that the observation network used in this study is capable of providing adequate resolution to constrain the slip distribution beneath the Himalaya.

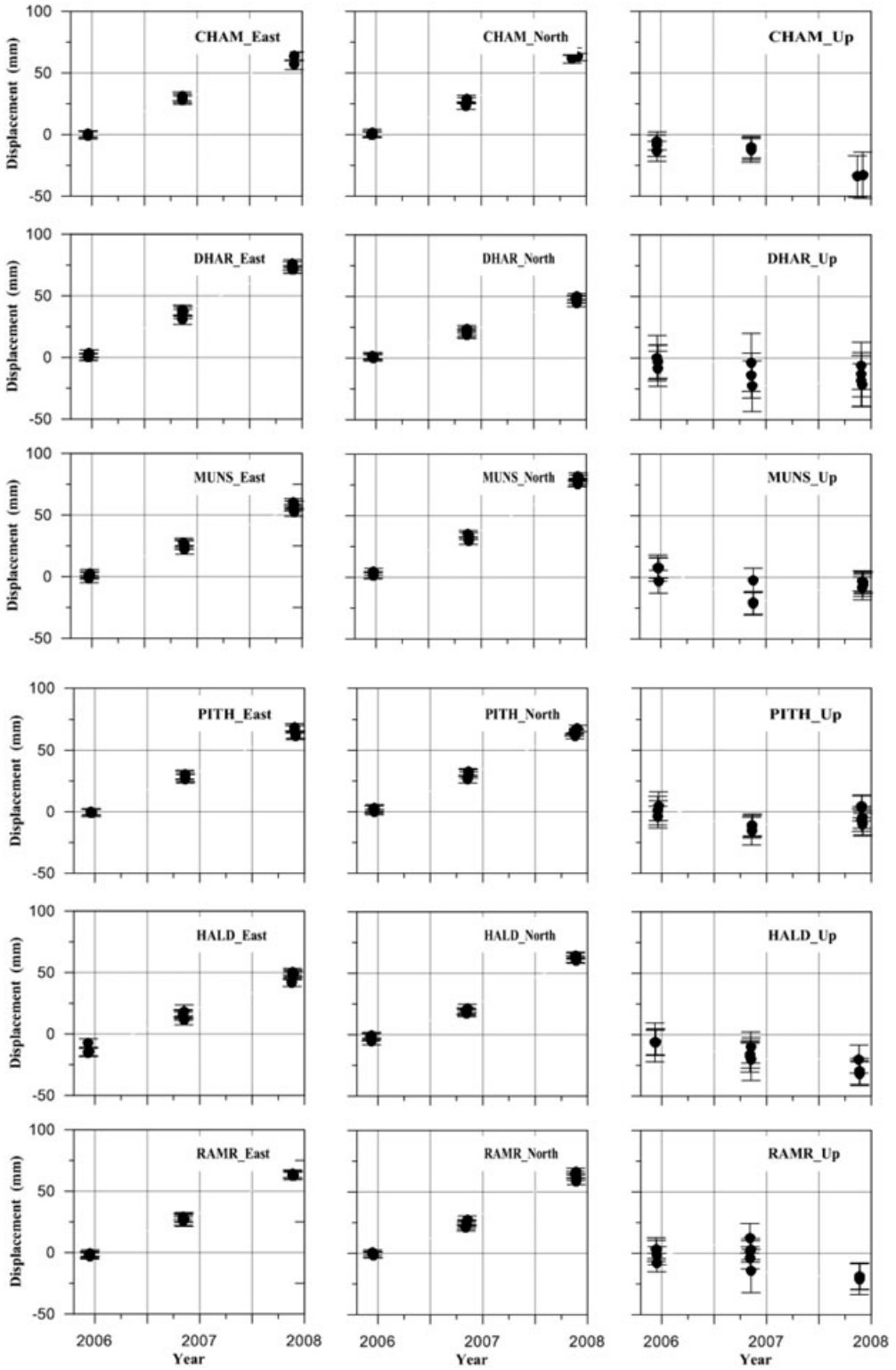

Figure 4. Time-series of GPS station velocities. The eastward, northward and upward components are presented along with the uncertainty.

4 INVERSION RESULTS

Fig. 9(a) explains the slip distribution beneath the Kumaun–Garhwal region of the Western Himalaya. The profiles (a–a′ and c–c′; Fig. 9c) of slip rate are a function of depth, and this may be the cause of structural detachment between the Kumaun and Garhwal Himalaya. Past studies (Ni & Barazangi 1984; Srivastava & Mitra 1994) involving well log and earthquake data have indicated that this region is underlain by a basal detachment fault dipping gently to the north at an angle of ∼2° and a depth of ∼20 km. The profile (b–b′) shows a lower slip rate in the plot of slip versus depth, probably because of less data in that section. The model reproducibility is

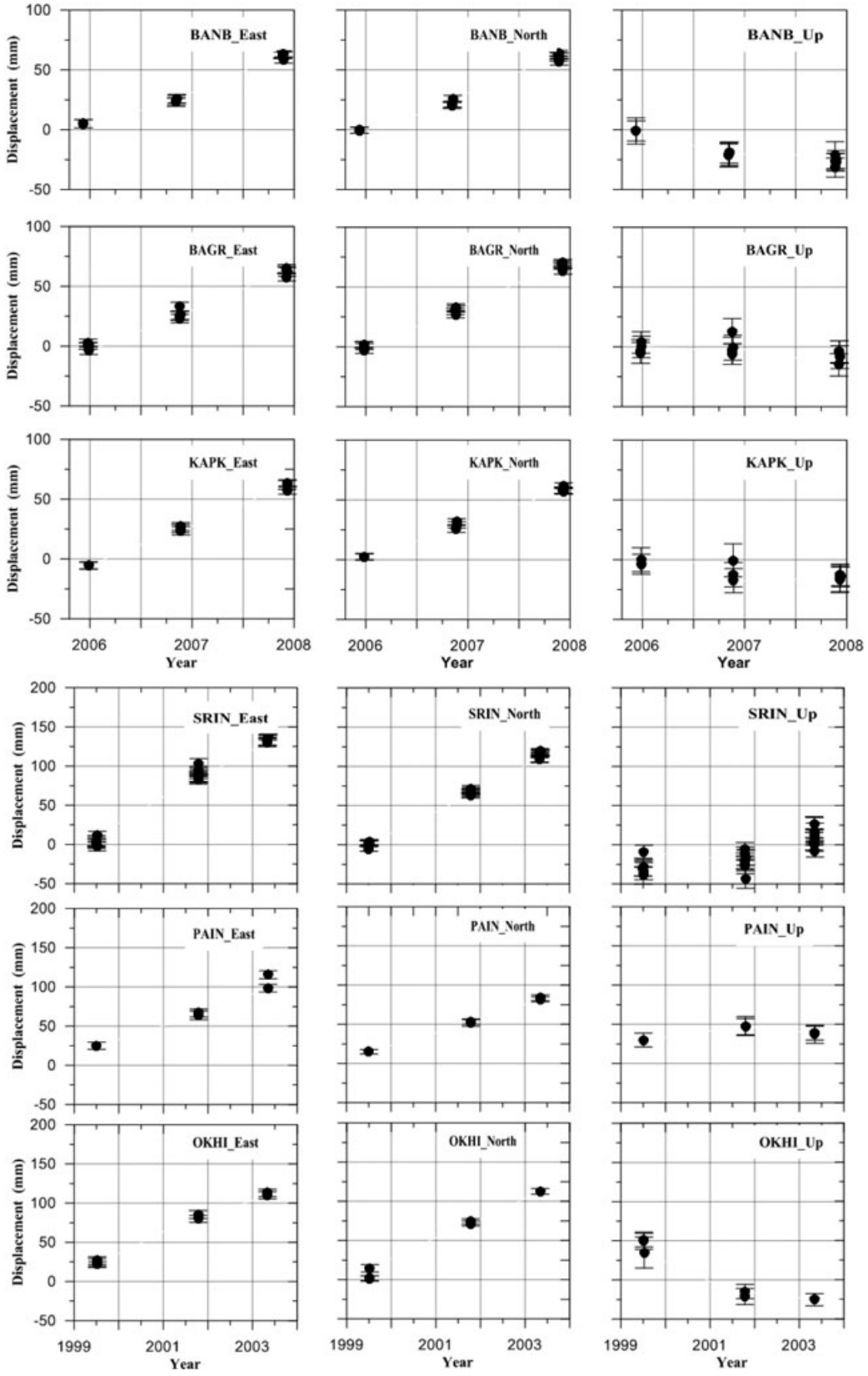

Figure 4. (*Continued.*)

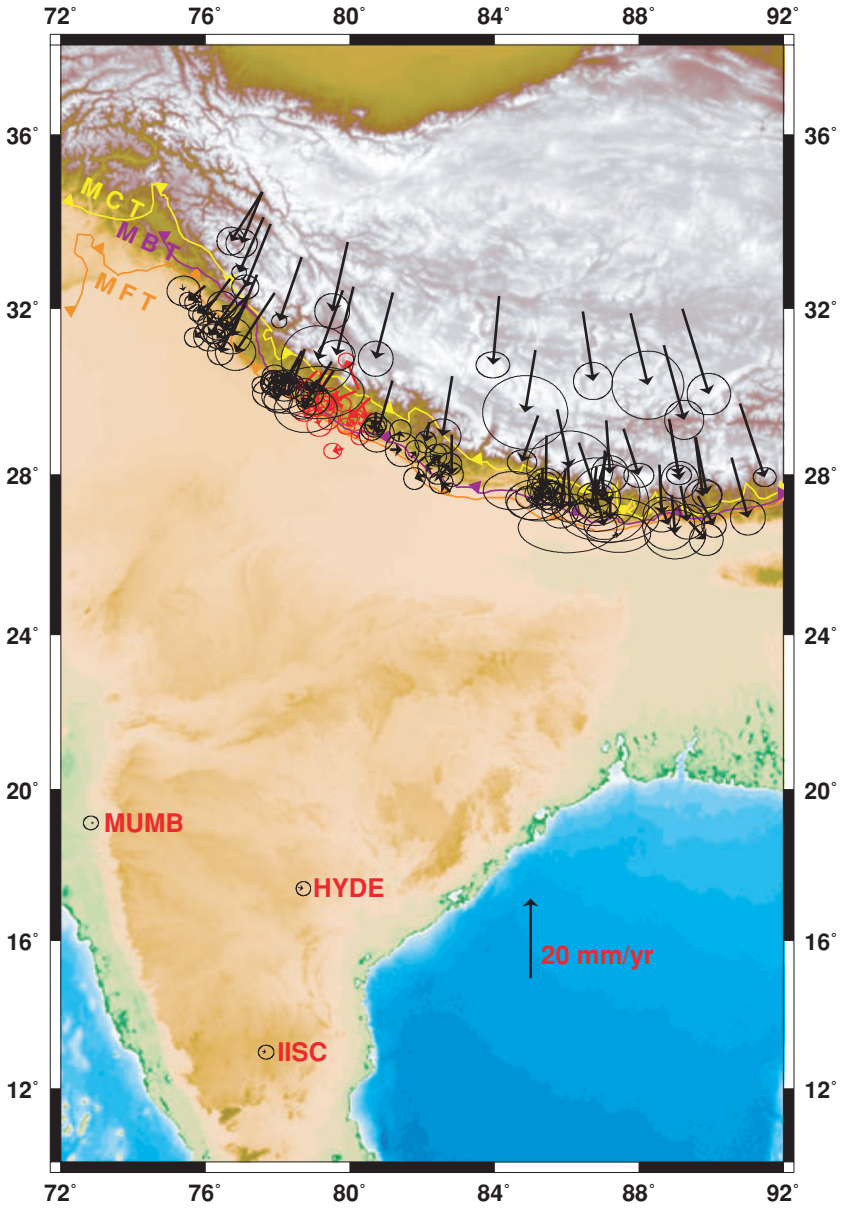

Figure 5. Estimated site velocities at GPS stations together with 95 per cent confidence error ellipses with respect to the fixed Indian frame. Red and black arrows denote the velocities obtained by this study and Banerjee *et al.* (2008), respectively. The lines with triangles denote the Main Central Thrust (MCT), Main Boundary Thrust (MBT) and Main Frontal Thrust (MFT).

shown in Fig. 9(b). Fig. 10(a) shows the optimum slip distribution obtained using the non-negative least-squares algorithms developed by Lawson & Hanson (1974); we assume a thrust-type dislocation on the grids. The model reproduces the overall site velocity pattern (Fig. 10b). Comparison of the model with the fault geometry (Fig. 10a) indicates a slip rate of 20 mm yr^{-1} in the fault depth range of 40–60 km. In the Central Himalaya and Western Himalaya, a creep motion of less than 10 mm is observed up to a depth of 30 km and 15 km, respectively. We infer that the Indian Plate is creeping in the deeper part of the frontal thrust fault, and this inference is consistent with that of earlier studies based on the dislocation model (Jouanne *et al.* 1999; Larson *et al.* 1999; Jouanne *et al.* 2004; Bettinelli *et al.* 2006). Bilham *et al.* (1997) have estimated the slipping rate of the Indian Plate to be ∼20 mm yr^{-1} at a depth of 20 km across the eastern Nepal Himalaya and at a depth of ∼25 km beneath western Nepal. The present model shows a low creeping rate (∼10 mm) at a depth of ∼30 km in the Nepal Himalaya. The MFT slip rate is estimated to be ∼14 mm yr^{-1} below a depth of 15 km in the Western Himalaya (Banerjee & Bürgmann 2002). It is also observed that the slip distribution in both the Central and Western Himalaya shows smooth variations, and a large slip rate (∼30 mm) is seen in the Central Himalaya at depths of 60–80 km.

5 DISCUSSION

The velocity field obtained in this study indicates that the collision zone in the study area is not deforming rapidly. For the observation period, the GPS stations distributed around the MFT and MBT do not indicate any deformation, while those in the region around the MCT suggest the occurrence of deformation. Similar deformation has previously been observed along the Nepal Himalaya by

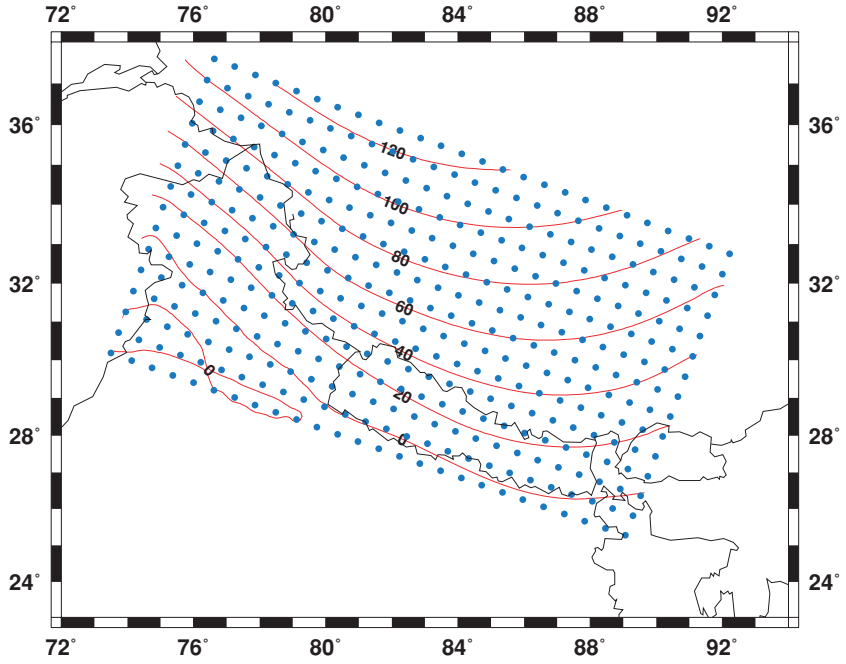

Figure 6. Fault geometry used for the geodetic inversion. The red lines are isodepth contours (unit: kilometre) of the plate boundary. The blue dots indicate grids on the fault plane, where the locations of thrust-type dislocations representing creep motion are determined.

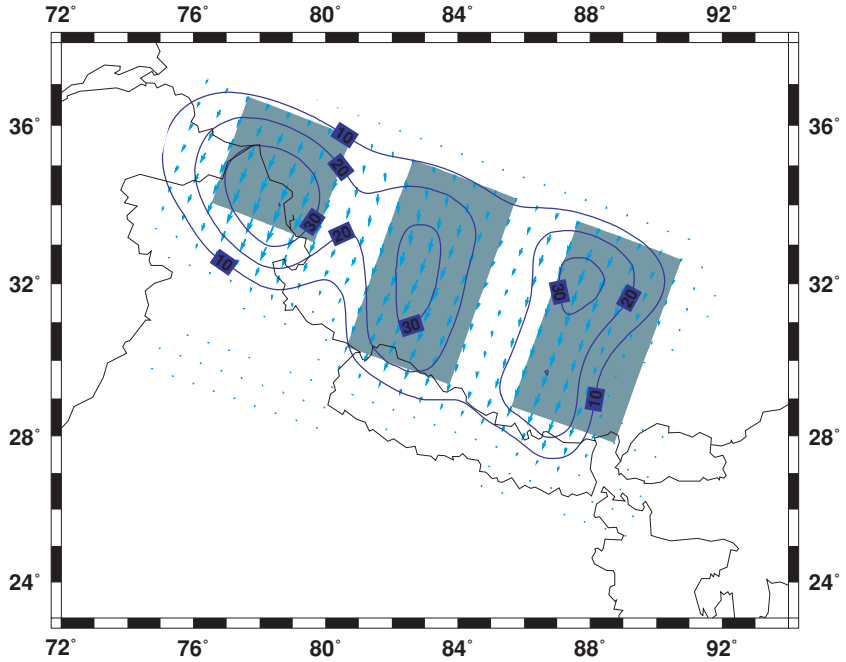

Figure 7. Slip patches grey (30 mm) and white (0 mm) were considered on the fault surface for the resolution test. The slip distribution (blue contour lines) derived by inversion is also shown.

using models of elastic strain accumulation for the region north of the locked Himalayan thrust system (Bilham *et al.* 1997; Larson *et al.* 1999). Focal mechanisms of earthquakes in the study region that occurred during the observation period are shown in Fig. 2; these earthquakes occurred to the north of the Himalaya and have been attributed to the thrust plane and the low-dip-angle strike plane (Bollinger *et al.* 2004; Jouanne *et al.* 2004). Slip vectors of thrust earthquakes that have occurred along the Higher Himalaya over the past few decades suggest that the earthquakes might have resulted from interseismic strains, because these events ruptured along shallow-dipping thrust faults (Pandey *et al.* 1995).

Profiles of the slip rate as a function of depth along 1–1′ to 5–5′ (Fig. 10c) are shown in Fig. 10(a). Profiles 1–3 are in the Central (Nepal) Himalaya, and 4 and 5 are in the Western Himalaya. The

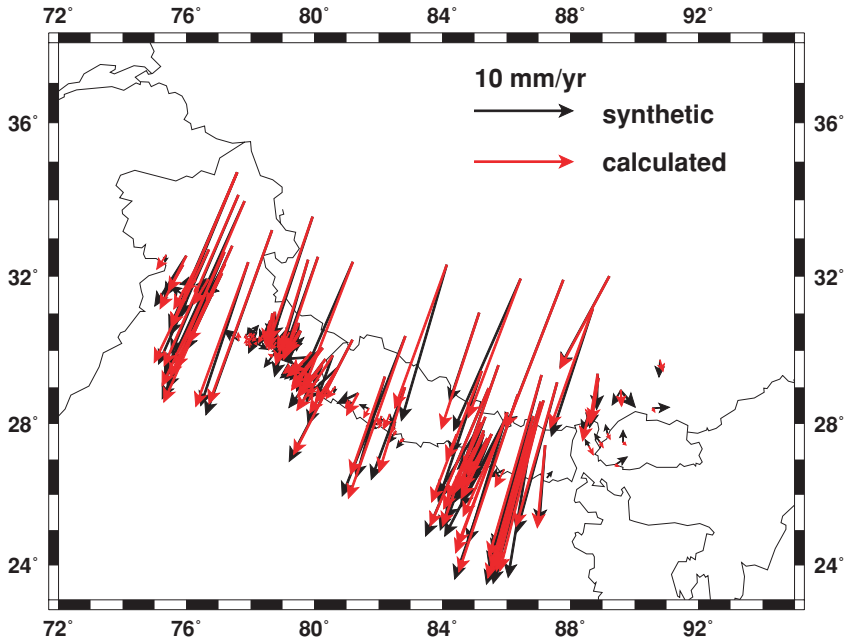

Figure 8. Comparison of synthetic and calculated velocities obtained in the resolution test.

overall profile shows a smooth distribution of the slip rate with respect to the depth, except for profile 1, which lies across eastern Nepal. There may be possible trade-off between the magnitude of slip and depth in the lower crust of the Central Himalaya, since high value of the slip magnitude obtained in the model. It is also clear that the Central Himalaya (profile 2–2′) shows differences in the structural anomaly in comparison to eastern and western Nepal. This suggests that the central Nepal segment (longitude: 82°–84°E) marks a discontinuity between eastern and western Nepal (Larson *et al.* 1999; Jouanne *et al.* 2004).

5.1 Comparison with seismicity

The Himalayan deformation is responsible for large earthquakes, and these earthquakes have ruptured the southern Himalayan arc (Seeber & Armbuster 1981; Pandey & Molnar 1988; Bilham *et al.* 2001), as shown in Fig. 2. A major portion of the current deformation is seen to lie between the Lesser and Higher Himalaya of the Kumaun–Garhwal region, which is coincides with the seismicity of the region (Fig. 3). This suggests that MCT is more active than MBT and basal detachment is present (Seeber *et al.* 1979; Ni & Barazangi 1984). A section of the plate boundary has not been ruptured over the last 300 yr (Bilham *et al.* 1997), and it is thought to be the location of great earthquakes. It is therefore necessary to evaluate the creep motion of the Indian Plate along the plate boundary. Recent earthquakes (Harvard CMT catalogue 2005–2007) along the plate boundary provide clues to the thrust and strike-slip mechanisms (Fig. 2). The seismicity in this region results mainly from the underthrusting of plates (Molnar *et al.* 1973; Ni & Barazangi 1984).

In the Nepal Himalaya, horizontal shortening due to ductile creep motion is observed along deep portions of the MFT, which is locked up to a depth of 20 km (Bettinelli *et al.* 2006). Along the strike of the Western Himalaya, the MFT is locked up to around 15 km (Banerjee & Bürgmann 2002). In our inversion model, we observe that the crust is creeping into the deep part of the MFT along the Nepal Himalaya and at shallower depths along the Western Himalaya. It is observed that the plate is creeping below 20 km and releasing elastic strain, which can cause minor to moderate earthquakes in the study region. Microseismic activities have been observed all along the Nepal Himalaya (Pandey *et al.* 1999), and it is being triggered by stress accumulation in the deep portion of the creeping zone (Cattin & Avouac 2000). Using our inversion technique, we have found that most of the historical large earthquake events have occurred in areas with slip velocities less than 10 mm yr^{-1}. Most of the earthquake events in this region are concentrated along the thrust zones and are confined to depths of about 20 km (Ni & Barazangi 1984).

6 CONCLUSION

We have attempted to explain the observed crustal deformation in the Himalaya in terms of coupling between the Indian and Eurasian Plates. GPS observations near the MCT indicate the presence of deformation, which is significant when considering the seismic activity in the thrust areas of the MCT. The regional crustal deformation is examined by analysing campaign-mode GPS data recorded in this study, apart from published data for the Nepal Himalaya and the northwest Himalaya. It is possible that there is a discontinuity in the structural fault between the Garhwal and Kumaun regions of Western Himalaya. We propose a model for the interplate coupling in the updip portion of the plate boundary. The model (NUC model) indicates that the shallow part (<20 km) of the thrust fault system along the plate boundary is almost locked. The locking depth appears to be large in the Central Himalaya and shallower in the Western Himalaya. The inferred location of the locked area matches with the locations of large earthquakes in the Himalaya.

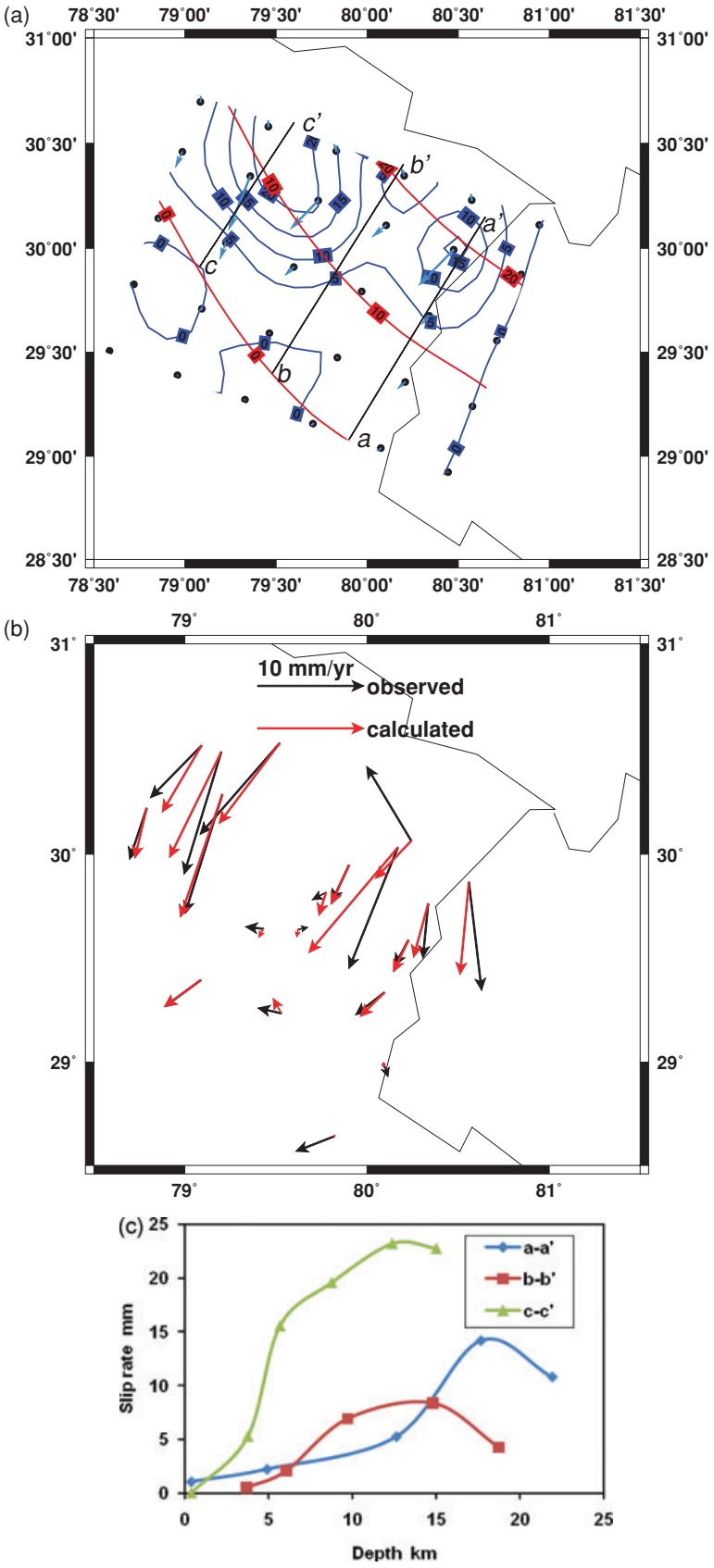

Figure 9. (a) Estimated slip distribution for the Kumaun–Garhwal region of Western Himalaya and contours are in millimetre per year. The black dots indicate the grid on the fault plane. The profiles (a–a′, b–b′ and c–c′) projected along the estimated slip are shown in Fig 8(c). (b) Calculated velocities and observed velocities for the slip distribution (Fig 8a). (c) Slip rate as a function of depth for the profiles (a–a′ to c–c′). [Correction made after online publication 2011 March 21: ′ symbol added to characters as needed in panel (a).]

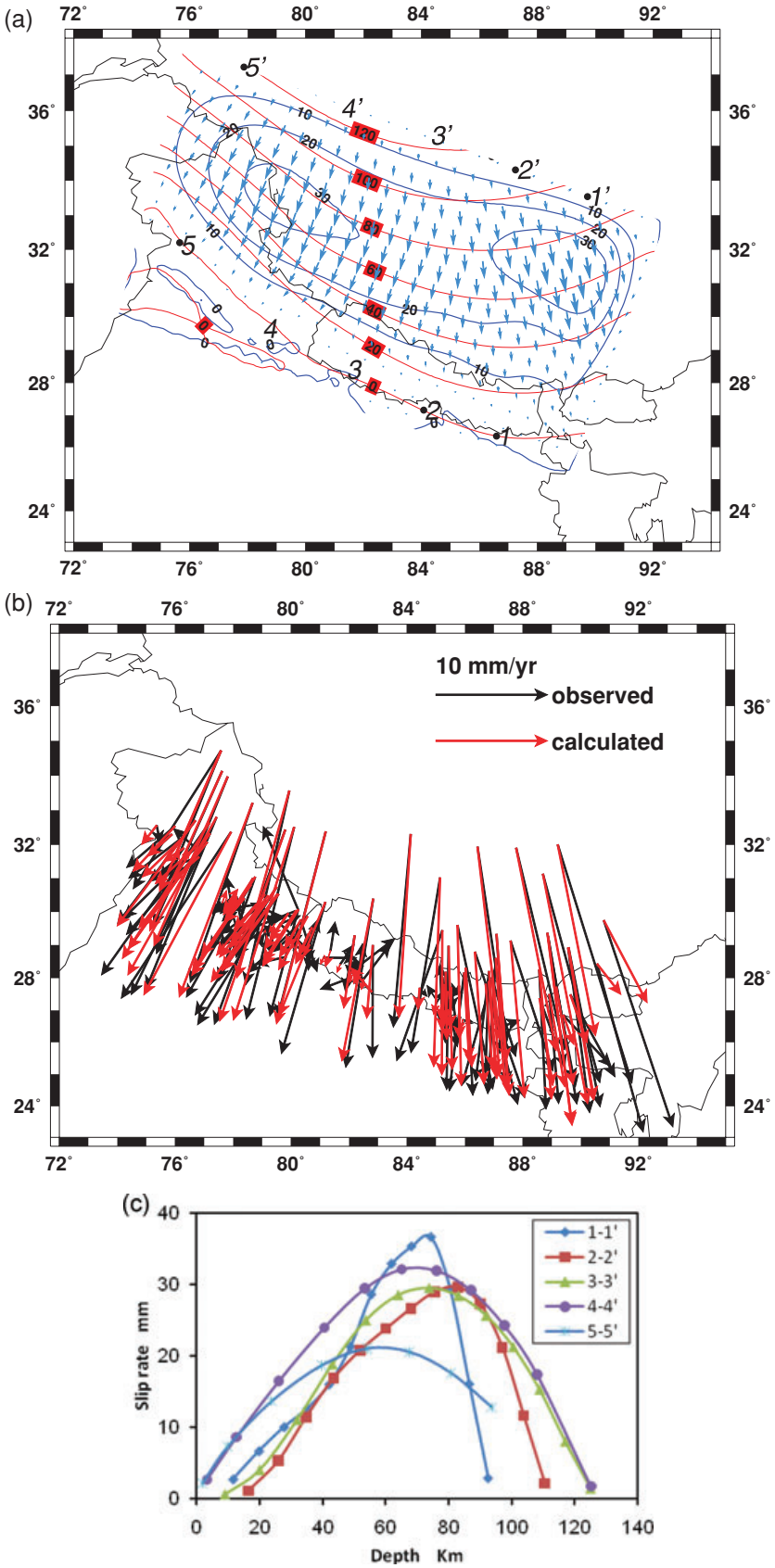

Figure 10. (a) Slip distribution on the fault (shown by the blue arrows). The contours indicate slip magnitudes in units of millimetre per year. The slip rate as a function of depth is projected along the profiles (1–1′ to 5–5′) in Fig. 9(c). (b) Comparison between observed (black arrows) and calculated (red arrows) site velocities. (c) Slip rate as a function of depth for the profiles (1–1′ to 5–5′). [Correction made after online publication 2011 March 21: ′ symbol added to characters as needed in panel (a).]

ACKNOWLEDGMENTS

We thank anonymous reviewers for constructive comments in improving the manuscripts. M. Ponraj (MP) conveys his sincere thanks to the Research Center for Predictions of Earthquakes and Volcanic Eruptions, Tohoku University, for providing him with excellent lab facilities. He is also grateful to the Japan Society for the Promotion of Science (JSPS), Japan, for providing financial support for his visits to Tohoku University, Sendai, Japan, and extends his sincere thanks to the Department of Science and Technology, New Delhi, for considering and recommending his application to the JSPS. We thank Dr. R. King for making the GAMIT/GLOBK GPS data analysis software available. We thank Prof. Mita Rajaram, Director, Indian Institute of Geomagnetism, Navi Mumbai, for encouragement and support. We also thank P. Wessel and W. H. F. Smith for the GMT software. We thank P. S. Sunil, S. K. Prajapati and K. Deenadayalan for their timely help.

REFERENCES

Altamimi, Z., Sillard, P. & Boucher, C., 2002. ITRF 2000: a new release of the international Terrestrial Reference Frame for Earth science applications, *J. geophys. Res.,* **107,** 2214, doi:1029/2001JB000561.

Ambraseys, N. & Bilham, R., 2000. A note on the Kangra $M_s = 7.8$ earthquake of 4 April 1905, *Curr. Sci.,* **79,** 45–50.

Armijo, R., Tapponnier, P., Mercier, J.L. & Tonglin, H., 1986. Quaternary extension in southern Tibet: field observations and tectonic implications, *J. geophys. Res.,* **91,** 13 803–13 872.

Banerjee, P. & Bürgmann, R., 2002. Convergence across northwest Himalaya from GPS measurements, *Geophys. Res. Lett.,* **29**(13), 301–304.

Banerjee, P., Bürgmann, R., Nagarajan, B. & Apel, E., 2008. Intraplate deformation of the Indian subcontinent, *Geophys. Res. Lett.,* **35,** doi:10.1029/2008GL035468.

Bettinelli, P., Avouac, J.P., Flouzat, M., Jouanne, F., Bollinger, L., Willis, P. & Chitraker, G.R., 2006. Plate motion of India and interseismic strain in the Nepal Himalaya from GPS and Doris measurements, *J. Geodyn.,* **80,** 567–589, doi:10.1007/s00190-006-0030-3.

Bilham, R., 1995. Location and magnitude of the 1833 Nepal earthquake and its relation to the rupture zones of contiguous great Himalayan earthquakes, *Curr. Sci.,* **69**(2), 155–187.

Bilham, R., Larson, K., Freymueller, J.T. & Project Idylhim members, 1997. GPS measurements of present-day convergence across the Nepal Himalaya, *Nature,* **386,** 61–64.

Bilham, R., Gaur, V.K. & Molnar, P., 2001. Himalayan seismic hazard, *Science,* **293,** 1442–1444.

Bollinger, L., Avouac, J.P., Cattin, R. & Pandey, M.R., 2004. Stress buildup in the Himalaya, *J. geophys. Res.,* **109,** B11405, doi:10.1029/2003JB002911.

Cattin, R. & Avouac, J.P., 2000. Modeling of mountain building and the seismic cycle in the Himalaya of Nepal, *J. geophys. Res.,* **105,** 13 389–13 407.

Chen, Q., Freymueller, J.T., Wang, Q., Yang, Z., Xu, C. & Liu, J., 2004a. A deforming block model for the present-day tectonics of Tibet, *J. geophys. Res.,* **109**(B1), B01403, doi:10.1029/2002JB002151.

Chen, Q., Freymueller, J.T., Yang, Z., Xu, C., Jiang, W., Wang, Q. & Liu, J., 2004b. Spatially variable extension in southern Tibet based on GPS measurements, *J. geophys. Res.,* **109**(B9), B09401, doi:10.1029/2002JB002350.

DeMets, C., Gordon, R.G., Argus, D.F. & Stein, S., 1994. Effect of recent revisions to the geomagnetic reversal time scale on estimates of current plate motions, *Geophys. Res. Lett.,* **21,** 2191–2194.

England, P. & Molnar, P., 1997. The field of crustal velocity in Asia calculated from Quaternary rates of slip on faults, *Geophys. J. Int.,* **130,** 551–582.

Feldl, N. & Bilham, R., 2006. Great Himalayan earthquakes and the Tibetan plateau, *Nature,* **444,** 165–170.

Gansser, A., 1964. *Geology of the Himalayas*. Interscience, London.

Hauck, M.L., Nelson, D., Brown, L.D., Zhao, W. & Ross, A.R., 1998. Crustal structure of the Himalayan orogen at 90° east longitude from Project INDEPTH deep reflection profiles, *Tectonics,* **17,** 481–500.

Herring, T.A., 2002. *GLOBK Global KALMAN Filter VLBI and GPS Analysis Program,* version 10.0. Mass. Inst. Technolog, Cambridge.

Holt, W.E., Chamot-Rooke, N., Le Pichon, X. & Haines, A.J., 2000. Velocity field in Asia inferred from Quaternary fault slip rates and Global Positioning System observations, *J. geophys. Res.,* **105,** 19 185–19 209.

Jade, S. *et al.*, 2004. GPS measurements from the Ladakh Himalaya, India: preliminary tests of plate-like or continuous deformation in Tibet, *GSA Bull.,* **116,** 1385–1391.

Jouanne, F. *et al*., 1999. Oblique convergence in the Himalayas of Western Nepal deduced from preliminary results of GPS measurements, *Geophys. Res. Lett.,* **26**(13), 1933–1936.

Jouanne, F. *et al*., 2004. Current shortening across the Himalayas of Nepal, *Geophys. J. Int.,* **157,** 1–14.

King, R.W. & Bock, Y., 2005. *Documentation for the GAMIT GPS Analysis Software, Release 10.2,* Massachusetts Institute of Technology, Cambridge, MA.

Khan, P.K. & Chakaraborthy, P.P., 2007. The seismic b-value and its correlation with Bouguer gravity anomaly over the Shillong plateau area: tectonic implications, *J. Asian Earth Sci.,* **29,** 136–147.

Khattri, K.N., 1987. Great earthquakes, seismicity gaps and potential for earthquakes along the Himalayan plate boundary, *Tectonophysics,* **38,** 79–92.

Larson, K.M., Burgmann, R., Bilham, R. & Freymueller, J.T., 1999. Kinematics of the India-Eurasia collision zone from GPS measurements, *J. geophys. Res.,* **104,** 1077–1093.

Lav'e, J. & Avouac, J.P., 2000. Active folding of fluvial terraces across the Siwaliks Hills, Himalayas of central Nepal, *J. geophys. Res.,* **105,** 5735–5770.

Lawson, C.L. & Hanson, R.J., 1974. *Solving least squares,* Prentice-Hall, Englewood Cliffs, NJ.

Lyard F., Lefevre F., Letellier T. & Francis O., 2006. Modelling the global ocean tides: a modern insight from FES2004, *Ocean Dyn.,* **56,** 394–415.

McClusky, S.M. *et al*., 2000. Global Positioning System constraints on plate kinematics and dynamics in the eastern Mediterranean and Caucasus, *J. geophys. Res.,* **105,** 5695–5719.

Molnar, P. & Tapponnier, P., 1977. The collision between India and Eurasia, *Sci. Am.,* **236,** 30–41.

Molnar, P. & Deng, Q., 1984. Faulting associated with large earthquakes and the average rate of deformation in central and eastern Asia, *J. geophys. Res.,* **89,** 6203–6227.

Molnar, P. & Lyon-Caen, H., 1989. Fault plane solutions of earthquakes and active tectonics of the Tibetan plateau and its margins, *Geophys. J. Int.,* **99,**123–153.

Molnar, P., Fitch, T.J. & Wu, F.T., 1973. Fault plane solutions of shallow earthquakes and contemporary tectonics in Asia, *Earth planet. Sci. Lett.,* **16,** 101–112.

Nakata, T., 1989. Active faults of the Himalayas of India and Nepal, *Geol. Soc. Am. spec.,* **232,** 243–264.

Nelson, K.D. *et al*., 1996. Partially molten middle crust beneath southern Tibet: synthesis of project INDEPTH results, *Science,* **274**(5293), 1684–1688.

Ni, J. & Barazangi, M., 1984. Seismotectonics of the Himalayan collision zone: geometry of the underthrusting Indian Plate beneath the Himalaya, *J. geophys. Res.,* **89,** 1147–1163.

Okada, Y., 1985. Surface deformation due to shear and tensile faults in a half-space, *Bull. seism. Soc. Am.,* **75,** 1135–1154.

Pandey, M.R. & Molnar, P., 1988.The distribution of Intensity of the Bihar Nepal earthquake of 15 January 1934 and bounds on the extent of the rupture, *J. Nepal Geol. Soc.,* **5,** 22–44.

Pandey, M.R., Tandukar, R.P., Avouac, J.P., Lavè, J. & Assot, J.P., 1995. Interseismic strain accumulation on the Himalaya crustal ramp (Nepal), *Geophys. Res. Lett.,* **22,** 741–754.

Pandey, M.R., Tandukar, R.P., Avouac, J.P., Vergne, J. & Hèritier, T., 1999. Seismotectonics of Nepal Himalayas from a local seismic network, *J. Asian Earth Sci.,* **17,** 703–754.

Patriat, P. & Achache, J., 1984. India-Eurasia collision chronology has implications for crustal shortening and driving mechanisms of plates, *Nature,* **311,** 615–621.

Seeber, L. & Armbruster, J.G., 1981. Great detachment earthquakes along the Himalayan Arc and long term forecasting, in *Earthquake Prediction: An International Review,* Vol. 4, pp. 259–277, eds Simpson, D.W. & Richards, P.G. Maurice Ewing Series, AGU, Washington, D.C.

Seeber, L., Quittmeyer, R. & Armbruster, J.G., 1979. Seismotectonics of Pakistan: a review of results from network data and importance for the central Himalaya, in *Structural Geology of the Himalayas,* pp. 361–392, ed. Saklani, P.S., Today's and Tomorrow's Publishers, New Delhi, India.

Seeber, L., Armbruster, J.G. & Quittmeyer, R.C., 1981. Seismicity and continental subduction in the Himalayan arc, in Zagros, *Hindu Kush Himalaya Geodynamic Evolution,* Vol. 3, pp. 215–242, eds Gupta, H.K. & Delany, F.M., Geodynamics Ser., AGU, Washington, D.C.

Srivastava, P. & Mitra G., 1994. Thrust geometries and deep structure of the outer and lesser Himalaya, Kumaun and Garhwal (India): implications for evolution of the Himalayan fold-and-thrust belt, *Tectonics,* **13,** 89–109.

Tsapanos, T.M., 1990. b-values of two tectonic parts in the Circum Pacific belt, *Pure appl. Geophys.,* **134,** 229–242.

Vergne, J., Cattin, R. & Avouac, J.P., 2001. On the use of dislocations to model interseismic strain and stress build-up at intracontinental thrust faults, *Geophys. J. Int.,* **147,** 155–162.

Vergnolle, M., Bouin M.-N., Morel, L., Masson, F., Durand, S., Nicolas, J. & Melachroinos, S., 2008. GPS estimates of ocean tide loading in NW-France: determination of ocean tide loading constituents and comparison with a recent ocean tidal model, *Geophys. J. Int.,* **173,** 444–458.

Wallace, L.M., Beaven, J., McCaffrey, R. & Darby, D., 2004. Subduction zone coupling and tectonic block rotations in the North Island, New Zealand, *J. geophys. Res.,* **109,** B12406, doi:10.1029/2004JB003241.

Wang, Q. *et al*., 2001. Present-day crustal deformation in China constrained by Global Positioning System measurements, *Science,* **294,** 574–577.

Wason, H.R., Sharma, M.L., Khan, P.K., Kapoor, K., Nandini, D. & Kara, V., 2002. Analysis of aftershocks of the Chamoli Earthquake of March 29, 1999 using broadband seismic data, *J. Himalayan Geol.,* **23,** 7–18.

Yabuki, T. & Matsu'ura, M., 1992. Geodetic data inversion using a Bayesian information criterion for spatial distribution of fault slip, *Geophys. J. Int.,* **109,** 363–375.

Yin, A., 2006. Cenozoic tectonic evolution of the Himalayan orogen as constrained by along-strike variation of structural geometry, exhumation history and foreland sedimentation, *Earth-Sci. Rev.,* **76,** 1–131.

Zhao, W., Nelson, K.D. & project INDEPTH Team, 1993. Deep seismic-reflection evidence continental underthrusting beneath southern Tibet, *Nature,* **366**(6455), 557–559.